Nanoscale

PAPER

View Article Online
View Journal | View Issue

Cite this: *Nanoscale*, 2022, **14**, 12757

Five-fold symmetry in Au–Si metallic glass†

Chang-Chun He,[a,b] Shao-Gang Xu,[a] Shao-Bin Qiu,[b] Chao He,[a] Yu-Jun Zhao,[b] Xiao-Bao Yang *[b] and Hu Xu *[a,c]

Received 30th May 2022,
Accepted 6th August 2022

DOI: 10.1039/d2nr02975h

rsc.li/nanoscale

The first metallic glass of Au–Si alloy for over half a century has been discovered, but its atomic structure is still puzzling. Herein, Au_8Si dodecahedrons with local five-fold symmetry are revealed as building blocks in Au–Si metallic glass, and the interconnection modes of Au_8Si dodecahedrons determine the medium-range order. With dimensionality reduction, the surface ordering is attributed to the motif transformation of Au_8Si dodecahedrons into planar Au_5Si pyramids with five-fold symmetry, and thus the self-assembly of Au_5Si pyramids leads to the formation of the ordered Au_2Si monolayer with the lowest energy. Furthermore, structural similarity analysis is performed to unveil the physical origin of the structural characteristics in different dimensions. The amorphism of Au–Si is due to the smooth energy landscape around the global minimum, while the ordered surface structure occurs due to the steep energy landscape.

Gold–silicon alloys were the first reported metallic glass, discovered in 1960 by rapid cooling.[1] Subsequently, bulk metallic glasses (BMGs) have attracted increasing attention due to their fundamental scientific interests and practical applications.[2–4] Up to now, many computational methods and experimental techniques have been involved to investigate structures of BMGs.[5–7] However, due to the absence of long-range order it remains challenging to determine atomic structures of BMGs.[8] For example, a combination of experimental measurements and reverse Monte Carlo modeling have failed to reproduce the precise packing structures of BMGs at the atomic level without sufficient structural information.[9] Numerous structural models have been proposed to improve the understanding of short-range order (SRO) in BMGs over the years,[10,11] but these models are still difficult to apply to figuring out the medium-range order (MRO) of BMGs.[12] To overcome this challenge, efficient cluster packing on a face-centered cubic lattice has been proposed.[13] In 2009, the MRO in BMGs was described by the packing mode of local motifs on a network with fractal dimension (D_f = 2.32),[14] which is smaller than that of crystals (D_f = 3.0) or dodecahedron-quasicrystals (D_f = 2.72), indicating that filling the real space in these amorphous solids by building blocks is impossible. Therefore, unveiling the nature of atomic packing at the MRO scale in BMGs[15] is a long-standing problem.

The Au–Si eutectic alloy has an extremely low eutectic temperature (359 °C), well below the melting points of Au (1063 °C) and Si (1412 °C).[16] At the lowest eutectic temperature, it has the composition $Au_{82}Si_{18}$,[16] which is key to the catalytic growth of silicon nanowires[17] because Si atoms maintain relatively high mobility at low temperatures.[18] In recent years, although some theoretical studies have reported possible alloy structures of Au–Si,[19–21] the local ordering of Au–Si BMGs is still lacking. Interestingly, two-dimensional (2D) crystallization was observed at the surface of Au–Si metallic glass,[22,23] which has been experimentally confirmed to be an ordered rectangular structure[22] with the proposed Si–Si bond on the surface. Shpyrko and co-workers[22] claimed that the Au–Si surface ordering was induced by surface-induced freezing,[24] but the ordered prefreezing surface will only appear near the transition temperature rather than a wide range of temperatures, inconsistent with the case of Au–Si. Moreover, density functional theory (DFT) calculations proved that the Si–Si bond is energetically unfavorable in the Au–Si alloy,[18,20] showing the inconsistency in the literature. This ordered surface plays a key role in crystal growth and solidification,[25,26] but the atomic arrangement is still unclear. Therefore, uncovering the atomic structures of surface crystallization and Au–Si alloy will be beneficial for understanding the exotic properties of Au–Si metallic glass.

In this article, *ab initio* molecular dynamics (AIMD) simulations were performed to investigate the bonding features of Au–Si in the undercooled state. The partial distribution function and coordination number analysis were employed to

[a]*Department of Physics, Southern University of Science and Technology, Shenzhen 518055, China. E-mail: xuh@sustech.edu.cn*
[b]*Department of Physics, South China University of Technology, Guangzhou 510640, China. E-mail: scxbyang@scut.edu.cn*
[c]*Shenzhen Key Laboratory of Advanced Quantum Functional Materials and Devices and Department of Physics, Southern University of Science and Technology, China*
† Electronic supplementary information (ESI) available. See DOI: https://doi.org/10.1039/d2nr02975h

explore the SRO of liquid Au–Si alloy, and a set of Au_8Si dodecahedrons with local five-fold symmetry are the most energetically favorable motifs. The connection modes of different Au_8Si motifs with similar energies are substantial to reconstruct the Au–Si eutectic alloy, subtly affecting the structural stability of Au–Si. With dimensionality reduction, the basic building motifs, *i.e.*, Au_8Si dodecahedrons, are reduced to be Au_5Si pyramids, which are Si-centered pentagons with five-fold symmetry. This phenomenon is confirmed by a systematic investigation of surface structures on the Au–Si alloy. Moreover, a 2D ordered Au_2Si monolayer composed of Au_5Si pyramids is found, which is more energetically favorable compared with all the earlier proposed surface structures. Notably, the simulated scanning tunneling microscopy (STM) images are in much better agreement with the experimental results. Furthermore, the remarkable difference of structural similarity between the Au–Si bulk and surface structures is uncovered, providing insights into understanding why the bulk structure is a metallic glass while the surface alloy exhibits long-range order.

1. Results and discussion

To extract the inherent local SRO of $Au_{82}Si_{18}$, the initial configurations were constructed based on the Au bulk in thermal equilibrium, where a certain number of Au atoms were randomly replaced with Si atoms. To avoid the systematic error, 100 configurations were used to produce structural information, for instance, the average coordination numbers and the partial pair-correlation functions (see the details in the section of computational methods in the ESI†). As shown in Fig. 1(a), the partial pair-correlation functions $g_{ij}(r)$ of $Au_{82}Si_{18}$ were obtained after the under-cooling process, where the simulation temperatures were quickly reduced to 300 K from 2000 K with a large cooling rate of 1×10^{11} K s^{-1}. The first peak of Au–Si is located at around 2.45 Å, suggesting intensive mixing between Au and Si atoms. The first broad peak of Si–Si appears around 4 Å, showing that Si atoms are prohibited from being bonded together and are surrounded by Au atoms. This phenomenon implies the existence of close packing that holds Si atoms like "solute" atoms in the center of polyhedrons. The coordination number (CN) analysis reveals that Au_8Si polyhedrons are the most frequent motifs in the Au–Si BMG, where the ratio reaches up to 79%, as shown in Fig. 1(b). It is worth noting that the frequent Au_8Si motifs have local five-fold symmetry in Fig. 1(c), which is responsible for the SRO. The ratio for these four motifs is 28.6%, 21.2%, 15.5%, 13.7%. As a result, we can infer that the atomic structure of the Au–Si alloy is the self-assembly of Au_8Si dodecahedrons by connecting each other in a close-packed manner.

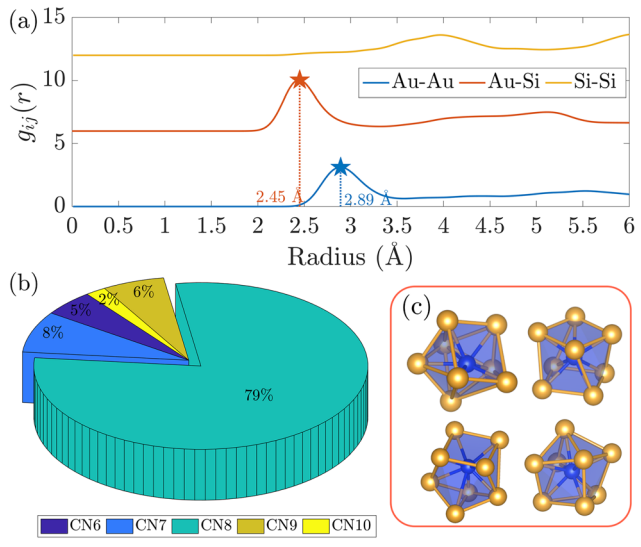

Fig. 1 (a) The pair-correlation functions of $Au_{82}Si_{18}$ BMG at room temperature. For clarification, the Si–Si and Au–Si partials are shifted by 5 and 10, respectively. (b) The coordination number distribution of $Au_{82}Si_{18}$ BMG at room temperature. (c) The most frequent Au_8Si motifs in $Au_{82}Si_{18}$ BMG.

The Au–Si and Au–Au pair-correlation functions induce shoulder peak splitting of the total pair-correlation function, indicating that the medium-range order is significant to characterize the ordering of Au–Si metallic glass.[27] To determine the MRO in Au–Si, we need to reveal the origin of its structural stability, where the building blocks and connection rules are crucial to identify the local atomic ordering. According to the bonding features we obtained in Fig. 1(a) and (b), we constructed a series of Au–Si configurations, which contain Au_nSi (n = 6–10) polyhedrons in a corner-sharing or edge-sharing mode, to explore stable structures of Au–Si alloy. As shown in Fig. 2(a), the Au_4Si structure has the lowest formation energy, which is in excellent agreement with the eutectic point of the Au–Si phase diagram.[16] Particularly, two stable structures with almost the same energy have been found, which are both comprised of Au_8Si motifs in body-centered cubic (see Fig. 2(b)) and hexagonal close-packed (see Fig. 2(c)) structures. Moreover, we find that these two Au_8Si motifs can be combined together to form relatively stable structures with a larger number of atoms (see Fig. 2(d)), indicating that the connection modes are not dominant for the structural stability of Au–Si compared to the local atomic ordering. Therefore, the MRO at the atomic level is ascribed to the interconnection modes of Au_8Si motifs. It is worth noting that the formation energy distribution at a Au concentration of 0.8 is very close, implying a flat energy landscape and the origin of formation mechanism in Au–Si.[28]

The Au_8Si dodecahedrons with local five-fold symmetry are found to be the SRO in Au–Si, but with dimensionality reduction the SRO of surface structures is still unknown. The surface crystallization of Au–Si BMG was observed in the last decade, however, the origin and atomic structure of the surface ordering are still in debate.[22,24,26] We carried out AIMD simulations at 650 K to study the Si content in a roughly 25 Å-thick $Au_{82}Si_{18}$ slab with six layers, and five different slab models were considered to reduce systematic errors. During AIMD simulations Si atoms migrate to the surface from the central region, resulting in the higher concentration of Si

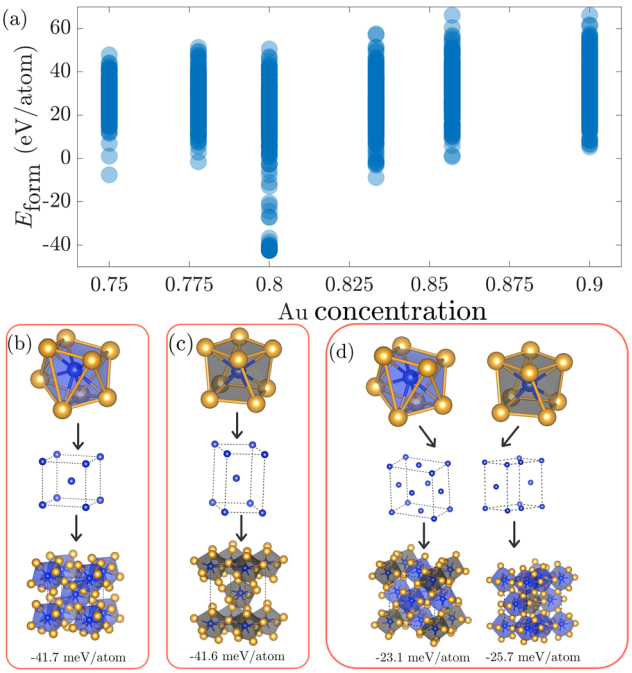

Fig. 2 (a) The formation energy of Au–Si alloy with various Au concentrations. (b and c) The most stable Au_4Si crystal structures, which are constructed by the fundamental Au_8Si motifs with different corner sharing modes. (d) The structure constructed from the two fundamental Au_8Si motifs with other corner sharing modes. Si and Au atoms are represented by blue and golden spheres, respectively.

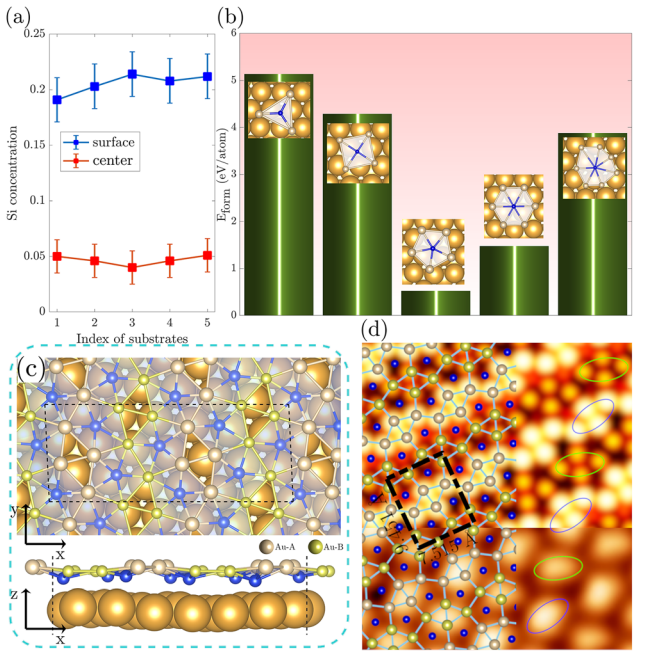

Fig. 3 (a) The concentration of Si atoms in the surface layer and central region for five different slab models. (b) Formation energy of one Si atom on the Au(111) substrate. The insets show the corresponding structure. (c) The top view and side view of the stable slab model. Surface Si atoms are represented by blue spheres, and the black dashed lines mark the lattice of the slab. (d) The simulated (upper) and experimental (bottom) STM images. The experimental STM image is reprinted with permission from Wiley VCH, 2019.[30]

atoms in the surface region. As shown in Fig. 3(a), the red line means there are only 5% Si atoms in the central layer, indicating the central layer is similar to Au(111) substrate. However, in the surface layer there are 23% Si atoms, implying the surface structure is roughly composed of $Au_{77}Si_{23}$. Therefore, our results agree with the fact that Si atoms prefer the surface segregation in experiments,[22] and the surface structure of Au–Si alloys represents the mixture of Au and Si atoms.

Interestingly, this ordered rectangular surface structure with the same lattice parameters has also been experimentally observed by depositing Si atoms on the Au(111) substrate.[29,30] Therefore, it is possible to search for the stable Au–Si surface structure on the Au(111) substrate. At the initial stage of the nucleation process, only one Si atom was introduced to react with the Au(111) substrate. The Au_nSi (n = 3–7) clusters with various coordination numbers for Si on Au(111) are shown in Fig. 3(b). It is apparent that the Au_5Si cluster with five-fold symmetry has the lowest formation energy, indicating that the Au_5Si pyramid is an energetically favorable motif in the Au–Si system.

To efficiently search for the possible structure of 2D Au–Si alloy, surface structure generation methods were employed to fertilize the structure database of Au–Si monolayers. We generated non-duplicated 2D Au–Si surface structures with various atomic ratios and distributions using the package Structures of Alloy Generation And Recognition (SAGAR)[31,32] and the crystal prediction algorithm RG2 based on space group theory and graph theory.[33] To consider the lattice mismatch between monolayers and Au(111), we constructed various supercells. High-throughput first-principles calculations were performed to determine the possible surface structure on Au(111). As shown in Fig. S1 of the ESI,† our results point out that Au–Si monolayers with Au_5Si pyramids are rather stable compared with those monolayers without Au_5Si pyramids, indicating that the Au_5Si motif with five-fold symmetry is the key SRO in surface structures of Au–Si.

The most stable Au–Si monolayer on Au(111) is Au_2Si comprised of pentagons and rhombuses, and the relaxed Au_2Si monolayer on Au(111) is shown in Fig. 3(c). Intriguingly, the lattice parameters of the most stable Au_2Si monolayer are a = 9.451 Å and b = 7.515 Å, which are in excellent agreement with previous experimental results.[22,29,30] Si atoms are at a lower height than Au atoms in the Au–Si monolayer, implying that each rhombus contains four Au atoms in the topmost layer and Si atoms are separated by these Au_4 rhombuses. In the experimental and simulated STM images shown in Fig. 3(d), the bright protrusions correspond to the Au_4 rhombuses. There are two types of protrusions in the Au_2Si monolayer that are rotated with respect to each other, as highlighted by the ellipses,[29] corresponding to the two types of Au atoms at different heights in Fig. 3(c). The Au_5Si pyramids reflect dark pores in the STM image because the Si atoms are at a relatively

low height. Therefore, we conclude that the Au_2Si monolayer forms by depositing Si atoms on the Au(111) substrate.

To further confirm the existence of the ordered Au_2Si monolayer at the surface of $Au_{82}Si_{18}$ BMG, various Au–Si overlayers were deposited on the five slab models mentioned above in Fig. 3(a). The calculated formation energies on these five substrates are shown in Fig. S2 of the ESI,† where the Au_2Si overlayer exhibits robust stability on different substrates, while other overlayers are less stable. This is strong evidence that the Au_2Si monolayer is the pretty stable ordered surface structure of Au–Si BMG.

The Au–Si BMG displays diverse structural characteristics in different dimensions, which is attributed to unusual Au–Si bonding properties and dimensionality reduction.[22] To unveil the deep physical nature of the phenomenon, the energy landscape of the Au–Si system is comprehensively investigated to uncover the origin of the distinction between bulk and surface. If the global minimum is surrounded by numerous local minima, namely, lots of low energy saddle points are around the ground state structure, this system is a glassy system, otherwise, it belongs to a structure seeker system.[28] For instance, the carbon and boron nitride systems can be clearly identified as structure seekers while the large boron cluster systems are glassy.[34]

To define the distance between any two structures, we employed the Smooth Overlap of Atomic Positions (SOAP) descriptor[35] to encode regions of atomic geometries using local expansion of Gaussian atomic density. The bulk Au–Si alloy and surface structures were generated by SAGAR and RG2 algorithms as mentioned above. We chose several low-energy Au–Si structures to perform the distance–energy analysis[36] in 2D and three-dimensional (3D) systems as shown in Fig. 4(a).

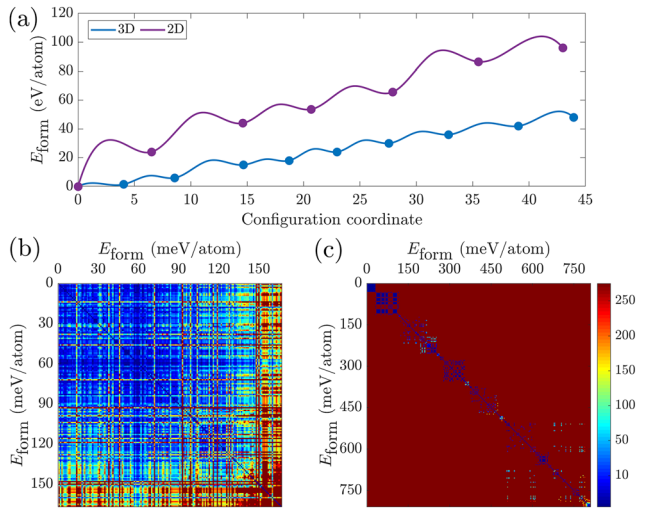

Fig. 4 (a) The distance–energy analysis for low-energy Au–Si structures in 2D and 3D systems. The structural similarity distribution in bulk and surface Au–Si are shown in (b) and (c), respectively. The colors represent the similarity degree between the two structures, where blue/red represents the small/large distance, corresponding to the shared colorbar on the right, which is applicable for both 3D and 2D systems.

For 2D surface structures, the formation energy increases quickly with configuration coordinate, and the saddle points are relatively far away from each other according to the configuration coordinate, compared with the case of 3D bulk structures. In the bulk case, the blue color in Fig. 4(b) shows that the distances among the low energy structures are rather small, indicating that there is a low energy barrier between two local minima. This feature leads to the fact that it is difficult to form any ordered bulk Au–Si alloy during the rapid cooling process, which has been confirmed by molecular dynamics simulations in Au–Si BMGs.[37] However, the image of the Au–Si surface structure (see Fig. 4(c)) is almost filled with the red color, implying that distances are much larger between the low and high energy structures. Therefore, long-range ordering can easily appear in surface structures.

2. Conclusions

In summary, we have uncovered the local ordering of Au–Si, where the Au_8Si motifs with local five-fold symmetry are the basic building blocks and the different connection modes reveal the MRO. With dimensionality reduction, the SRO of the Au–Si surface structure has been transformed into Au_5Si pyramids with five-fold symmetry. We have concluded that the Au_2Si monolayer composed of Au_5Si pyramids is the surface structure observed in experiments, due to the lowest formation energy and excellent agreement with STM images. Employing the structural similarity matrix based on the SOAP descriptor to metricize the distance among Au–Si structures, we have shown that there is a smooth energy landscape with dense local minima for the Au–Si bulk, while the energy landscape of the Au–Si surface structures is relatively steep around the ground state. Our work not only supplies a structure search method to determine the Au–Si structures in different dimensions but also expands on the intrinsic origin of the order–disorder transition in Au–Si alloy from 2D to 3D, which may provide a promising avenue to explore the novel properties in other metallic glasses.

Conflicts of interest

There are no conflicts to declare.

Acknowledgements

This work was supported by the Science, Technology, and Innovation Commission of Shenzhen Municipality (Grant No.s RCYX20200714114523069 and ZDSYS20190902092905285), the National Natural Science Foundation of China (No. 11974160), Guangdong Basic and Applied Basic Research Foundation (Grant No. 2021A1515010328), and Key-Area Research and Development Program of Guangdong Province (No. 2020B010183001). The Major Science and Technology Infrastructure Project of Material Genome Big-science

Facilities Platform supported by Municipal Development and Reform Commission of Shenzhen. The computer time at the Center for Computational Science and Engineering at Southern University of Science and Technology is gratefully acknowledged.

References

1 W. Klement, R. H. Willens and P. Duwez, *Nature*, 1960, **187**, 869–870.
2 T. Fujita, K. Konno, W. Zhang, V. Ku, M. Matsuura, A. Inoue, T. Sakurai and M. W. Chen, *Phys. Rev. Lett.*, 2009, **103**, 075502.
3 A. Inoue, *Acta Mater.*, 2000, **48**, 279–306.
4 A. Hirata, L. J. Kang, T. Fujita, B. Klumov, K. Matsue, M. Kotani, A. R. Yavari and M. W. Chen, *Science*, 2013, **341**, 376–379.
5 K. F. Kelton, G. W. Lee, A. K. Gangopadhyay, R. W. Hyers, T. J. Rathz, J. R. Rogers, M. B. Robinson and D. S. Robinson, *Phys. Rev. Lett.*, 2003, **90**, 195504.
6 A. Hirata, P. Guan, T. Fujita, Y. Hirotsu, A. Inoue, A. R. Yavari, T. Sakurai and M. Chen, *Nat. Mater.*, 2011, **10**, 28–33.
7 L. Zhong, J. Wang, H. Sheng, Z. Zhang and S. X. Mao, *Nature*, 2014, **512**, 177–180.
8 Y. Q. Cheng, E. Ma and H. W. Sheng, *Phys. Rev. Lett.*, 2009, **102**, 245501.
9 D. A. Keen and R. L. McGreevy, *Nature*, 1990, **344**, 423–425.
10 J. D. Bernal, *Nature*, 1960, **185**, 68–70.
11 P. H. Gaskell, *Nature*, 1978, **276**, 484–485.
12 H. W. Sheng, W. K. Luo, F. M. Alamgir, J. M. Bai and E. Ma, *Nature*, 2006, **439**, 419–425.
13 D. B. Miracle, *Nat. Mater.*, 2004, **3**, 697–702.
14 D. Ma, A. D. Stoica and X.-L. Wang, *Nat. Mater.*, 2009, **8**, 30–34.
15 D. B. Miracle, T. Egami, K. M. Flores and K. F. Kelton, *MRS Bull.*, 2007, **32**, 629–634.
16 H. Okamoto and T. B. Massalski, *Bull. Alloy Phase Diagrams*, 1983, **4**, 190–198.
17 J. B. Hannon, S. Kodambaka, F. M. Ross and R. M. Tromp, *Nature*, 2006, **440**, 69–71.
18 A. Pasturel, E. S. Tasci, c. H. F. Sluiter and N. Jakse, *Phys. Rev. B: Condens. Matter Mater. Phys.*, 2010, **81**, 140202.
19 E. S. Tasci, cel H. F. Sluiter, A. Pasturel and P. Villars, *Acta Mater.*, 2010, **58**, 449–456.
20 Y.-H. Dong, W.-C. Lu, X. Xu, X. Zhao, K. M. Ho and C. Z. Wang, *Phys. Rev. B*, 2017, **95**, 134109.
21 S.-H. Lee and G. S. Hwang, *J. Chem. Phys.*, 2007, **127**, 224710.
22 O. G. Shpyrko, R. Streitel, V. S. K. Balagurusamy, A. Y. Grigoriev, M. Deutsch, B. M. Ocko, M. Meron, B. Lin and P. S. Pershan, *Science*, 2006, **313**, 77–80.
23 G. Kurtuldu and J. F. Löffler, *Adv. Sci.*, 2020, **7**, 1903544.
24 B. Pluis, D. Frenkel and J. van der Veen, *Surf. Sci.*, 1990, **239**, 282–300.
25 D. Chatterjee, A. Annamareddy, J. Ketkaew, J. Schroers, D. Morgan and P. M. Voyles, *ACS Nano*, 2021, **15**, 11309–11316.
26 F. Panciera, J. Tersoff, A. D. Gamalski, K. C. Reuter, D. Zakharov, E. A. Stach, S. Hofmann and F. M. Ross, *Adv. Mater.*, 2019, **31**, 1806544.
27 K. Zhang, H. Li, L. Li and X. F. Bian, *Appl. Phys. Lett.*, 2013, **102**, 071907.
28 S. De, B. Schaefer, A. Sadeghi, M. Sicher, D. G. Kanhere and S. Goedecker, *Phys. Rev. Lett.*, 2014, **112**, 083401.
29 S. Sadeddine, H. Enriquez, A. Bendounan, P. Ku Das, I. Vobornik, A. Kara, A. J. ne, F. Sirotti, G. Dujardin and H. Oughaddou, *Sci. Rep.*, 2017, **7**, 44400.
30 A. Stpniak-Dybala, P. Dyniec, E. Kopciuszyski, R. Zdyb, M. Jałochowski and I. Krawiec, *Adv. Funct. Mater.*, 2019, **29**, 1906053.
31 C.-C. He, S.-B. Qiu, J.-S. Yu, J.-H. Liao, Y.-J. Zhao and X.-B. Yang, *J. Phys. Chem. A*, 2020, **124**, 4506–4511.
32 C.-C. He, J.-H. Liao, S.-B. Qiu, Y.-J. Zhao and X.-B. Yang, *Comput. Mater. Sci.*, 2021, **193**, 110386.
33 X. Shi, C. He, C. J. Pickard, C. Tang and J. Zhong, *Phys. Rev. B*, 2018, **97**, 014104.
34 S. De, A. Willand, M. Amsler, P. Pochet, L. Genovese and S. Goedecker, *Phys. Rev. Lett.*, 2011, **106**, 225502.
35 A. P. Bartók, R. Kondor and G. Csányi, *Phys. Rev. B: Condens. Matter Mater. Phys.*, 2013, **87**, 184115.
36 A. Sadeghi, S. A. Ghasemi, B. Schaefer, S. Mohr, K. A. Lill and S. Goedecker, *J. Chem. Phys.*, 2013, **139**, 184118.
37 C.-Y. Ran, L.-L. Zhou, Y.-C. Liang, Y.-F. Mo, Q. Chen, Z.-A. Tian, R.-S. Liu, T.-H. Gao and Q. Xie, *J. Non-Cryst. Solids*, 2021, **563**, 120787.